Ti/Au Die Backside Metallization for Flip Chip Heat Spreader Attachment

Yuquan Li, R. Wayne Johnson, *Fellow, IEEE*, Rui Zhang, Phillip Henson, Patrick Thompson, *Senior Member, IEEE*, Tejpal Hooghan, and Jeremias Libres

***Abstract*—In this paper, a heat spreader attachment with indium solder for high-power flip chip-in-package application was investigated. The Cu heat spreader was metallized with Ni/Au and the flip chip die backside metallization was Ti/Au. A low voiding attachment process was achieved with vacuum soldering. The Au thin film was converted into $AuIn_2$ completely after initial soldering, but no intermetallic compund (IMC) formation between Ti and In was observed. The attachment had good mechanical strength as measured by shear testing. The shear strength was not degraded significantly after multiple lead free solder reflows or with thermal aging at 120 °C. For thermal shock cycle test (−40 °C to 85 °C), die with Ti/Au (2000 Å of Au) metallization had early partial delamination. The effect of Au thickness on mechanical strength was further evaluated. Assemblies (Cu on Si) with Ti/Au (2000 Å) die had lower shear strength compared with Ti/Au (3000 Å) and Ti/Au (4000 Å) die. The pull strength (Si on Si) increased with increasing gold thickness. Thermal shock testing (−40 °C to 85 °C) for assemblies with Ti/Au 3000 Å along with Ti/Ni/Au (control) did not show early delamination and had similar performance after 2000 cycles.**

***Index Terms*—Flip chip in package, indium attachment, lid attachment.**

I. Introduction

INCREASES in speed and functionality of high-performance microprocessors and application-specific integrated circuits (ASICs) results in increased I/Os and power dissipation. The International Technology Roadmap for Semiconductors (ITRS) and the International Electronics Manufacturing Initiative predicted that "the absolute power levels in microelectronic devices will continue to increase above and beyond 100 W." [1]

Flip chip in package is commonly used to address the high I/O counts. This packaging method exposes the backside of the semiconductor die for heat removal. A high thermal conductivity heat spreader significantly larger than the Si die is typically attached to the back of the die to serve as a large area interface to the next level cooling hardware, usually a finned heat sink. The thermal interface material (TIM) between the die and heat spreader can be a filled organic or a metal.

Manuscript received June 16, 2009; revised September 26, 2009. Current version published January 07, 2010. This work was recommended for publication by Associate Editor I. Fidan upon evaluation of the reviewers comments.

Y. Li, R. W. Johnson, R. Zhang, and P. Henson are with the Electrical and Computer Engineering Department, Auburn University, Auburn, AL 36849 USA (e-mail: johnson@eng.auburn.edu).

P. Thompson, T. Hooghan, and J. Libres are with the Texas Instruments, Dallas, TX 75243 USA.

Color versions of one or more of the figures in this paper are available online at http://ieeexplore.ieee.org.

Digital Object Identifier 10.1109/TEPM.2009.2037012

Indium solder has been used as a TIM [2]–[7] for high power application (> 100 W), mainly because of its high thermal conductivity (82 W/mK) among solders and its low modulus. The In deforms under the stress caused by the coefficient of thermal expansion (CTE) mismatch between the Si die and the copper heat spreader [8]. Deppisch, *et al.* characterized indium based heat spreader attach [4]. Ti/NiV/Au was used as the Si backside metallization and Ni/Au was the surface finish for the heat spreader. After initial reflow assembly, $AuIn_2$ and $In_{72}Ni_{23}Au_5$ formed on the die side, while $AuIn_2$ and an In–Ni–Au intermetallic were identified at the interface to the heat spreader. After thermal cycling, the heat spreader intermetallic layer structure above the Ni was: Ni_2In_3, $(Ni, Au)_2In_3$ and $AuIn_2$. On the die side, the intermetallic layers after thermal cycling were $AuIn_2$ and $In_{72}Ni_{23}Au_5$. The $AuIn_2$ on the die side was discontinuous due to "the lower gold thickness on the die side and (it) disperses into the indium after solid-state elevated temperature exposure."[4]. Lid pull and failure analysis indicated the primary failure mode was between the $AuIn_2$ and the bulk In on the heat spreader side. Chaowasakoo, *et al.* demonstrated that the thickness of the $Ni_xAu_yIn_z$ intermetallic layer after reflow is a function of the Au thickness in the initial Ni/Au layers [7]. The continuous $Ni_xAu_yIn_z$ intermetallic layer increased in thickness as the Au thickness increased from thin to medium, then decreased as the Au thickness was further increased to thick (actual thicknesses were not given). The $AuIn_2$ layer was discontinuous, but increased in thickness with increasing initial Au thickness. A continuous Ni_xIn_y intermetallic layer was observed under the $Ni_xAu_yIn_z$ intermetallic layer.

The original question that initiated the present work was: "what is the minimum thickness of thin film Ni on the back side of the die required for reliability after multiple lead free reflows for package assembly at the next level and for high-temperature service life in the field?" The concern was the consumption of the Ni to form intermetallics. At the same time, the authors were evaluating a TaN/Ru/Au backside Si die metallization with indium solder die attach for a cryogenic application [9]. The attachment was evaluated for mechanical strength after multiple solder reflows and after high-temperature storage. There was no pull strength degradation after four reflows with a peak reflow temperature of 260 °C. After an initial decrease in average die shear strength of $\sim 20\%$ during the first 100 h of storage at 125 °C, the average shear strength remained constant through 1000 h at 125 °C. The question then became: "is Ni required?" In this paper, Ti/Au flip chip die backside metallization with different gold thicknesses was evaluated for indium solder based heat spreader attachment.

Fig. 1. X-ray image for assembly in a reflow oven showing voids (white areas) in the die attach. The die in the image is 22 mm × 22 mm.

Fig. 2. X-ray image for assembly with thermal compression bonder showing voids (white areas) in the die attach. The die in the image is 22 mm × 22 mm.

A. Low Voiding Assembly Process Development

Low voiding is desired for heat spreader attachment to maximize heat transfer. A 22 mm × 22 mm sandwich construction of Si/In/Si with the Si metallized with Ti/Ni/Au was used to evaluate different soldering processes (reflow, thermal compression bonding, and vacuum soldering). The indium preforms (50 μm thick) were purchased from Williams Advanced Materials. For reflow soldering in a Heller 1800 reflow oven, the profile ramped to 180 °C and was held for 200 s. Various weights were evaluated during assembly. An N_2 reflow environment was used with no flux. The resulting assemblies had significant voiding (Fig. 1). Reflow in air with an indium compatible RA flux applied by dip fluxing was also investigated and the voiding was worse. Others have recently optimized a flux based assembly process using flux jetting [5]. An SET thermocompression bonder was then evaluated for reflow bonding the assembly. The bonding tool temperature (165 °C, 180 °C, and 200°C) and bonding force (50, 100, 200 and 400 g) were varied. The resulting assemblies had significant voiding (Fig. 2). Vacuum soldering ($\sim 5 \times 10^{-5}$ torr) with a temperature profile

Fig. 3. X-ray image for assembly with vacuum soldering showing a few small voids (white areas) in the die attach. The die in the image is 22 mm × 22 mm.

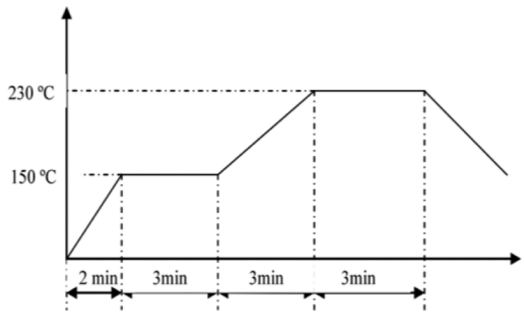

Fig. 4. Reflow temperature profile. The temperature is measured by a control thermocouple and is not the actual die attach joint temperature.

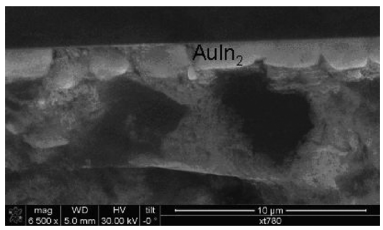

Fig. 5. Cross-section micrograph of Ti/(2000 Å) Au assembly showing $AuIn_2$ intermetallic.

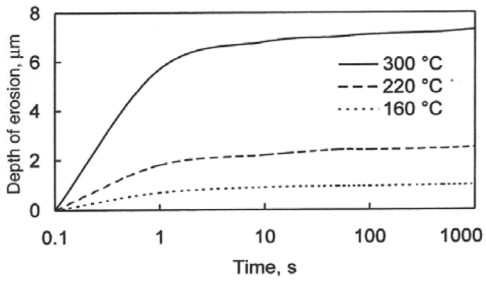

Fig. 6. Erosion rate of gold by molten indium [10].

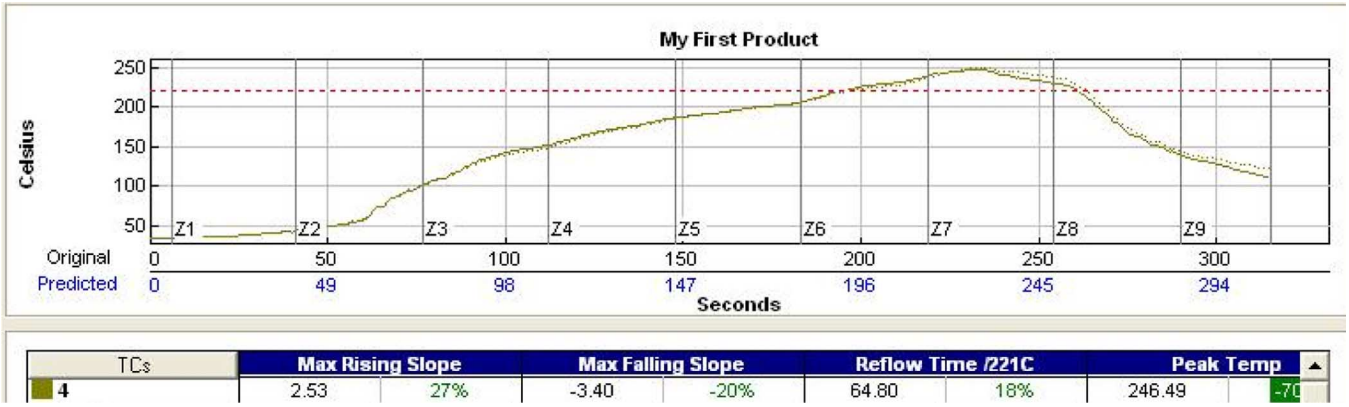

Fig. 7. Lead-free reflow temperature profile used to simulate subsequent thermal exposure of the lid attachment during package assembly to a printed circuit board.

dwell at 180 °C for 3 min and a 20-g weight yielded low voiding in the Si on Si assembly (Fig. 3).

For Cu heat spreader attachment, the flat 1-mm-thick copper heat spreaders used had a plated Ni (2.5–5 μm) finish as-supplied from the vendor. A 1000 Å Au layer was subsequently deposited by e-beam evaporation to enhance solderability. Before Au deposition, an *in situ* ion milling process was used to remove nickel oxide on the surface of the heat spreader.

The following vacuum soldering process was developed with good wetting and low voiding. For 10 mm × 10 mm Cu heat spreader on a 5 mm × 5 mm Si die assembly, a 1.3-g weight was used and for 24 mm × 24 mm Cu heat spreader on a 22 mm × 22 mm Si die, a 20 gram weight was used. Before assembly, the die and heat spreader were Ar plasma cleaned for 5 min. Fig. 4 shows the reflow temperature profile. The temperature measured is a reference temperature measured by the vacuum reflow system and not the actual In solder joint temperature. The vacuum was $\sim 5 \times 10^{-5}$ torr.

B. Heat Spreader Attachment With Ti/Au 2000 Å Metalized Die

Ti/Au2000 Å metallized Si was used for the initial experiments. 5 mm × 5 mm Si die were soldered on to 10 mm × 10 mm Si die. For all Ti/Au assemblies, the Ti thickness was 1000 Å. The solder joint microstructure was studied with scanning electron microscopy (SEM) and transmission electron microscopy (TEM). It was found that the gold thin film was consumed after initial soldering and completely converted to intermetallic (Fig. 5). The intermetallic was analyzed by X-ray energy dispersive spectroscopy (EDS) and determined to be 60–63at% In and 40–37at% Au, corresponding approximately to $AuIn_2$. Diffraction patterns from the intermetallic indicated a cubic crystal structure, consistent with $AuIn_2$. The complete consumption of the Au layer during the assembly thermal profile agrees with [10] (Fig. 6); however, the depletion of Au did not cause dewetting. The cross-sectional examination also showed that $AuIn_2$ was only at the interface—there were no $AuIn_2$ particles in the In layer as reported in [4], [7]. While Ti and In can form an intermetallic compund (IMC), energy dispersive spectroscopy (EDS) analysis did not detect any In–Ti intermetallic formation.

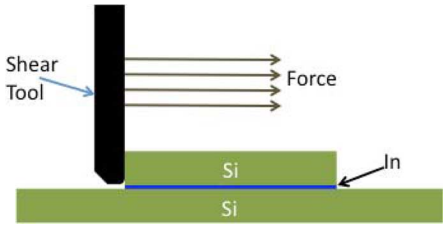

Fig. 8. Illustration of shear test. The force required to shear the top Si with respect to the bottom Si is measured.

The reliability of the heat spreader attachment with Ti/Au (2000 Å) die was examined. Si (5 mm × 5 mm)/In (5 mm × 5 mm × 50 μm)/Si (10 mm × 10 mm) assemblies were built and subjected to multiple reflows and thermal aging studies. With the move to lead-free solder for flip chip-in-package and package to printed circuit board assembly, the lead-free reflow profile shown in Fig. 7 was used to evaluate the In attachment as a function of exposure to lead-free reflow temperatures in subsequent assembly operations such as solder ball to package attachment and package to printed circuit board attachment. The peak temperature was 246 °C and the time above liquidus (221 °C) was 65 s. The shear strength was measured using a Dage PC2400 shear tester. The shear process is illustrated in Fig. 8. The shear speed was 6 μm/s. The die shear results as a function of reflows are plotted in Fig. 9. An ANOVA F-test was used to statistically evaluate the data [11]. At a 95% confidence level, there was, a mild statistical significance in shear strength as a function of reflow cycles ($F_{3/44} = 2.70$, P-value $= 0.0574$). There was a significant difference between the as-built samples and the mean of all reflowed (1x, 3x and 5x) samples ($F_{1/44} = 6.29$, P-value $= 0.0159$). Normality assumptions were confirmed using the Kolmogorov–Smirnov [12], [13], Cramer–von Mises [12], [13], and Anderson–Darling [13] tests as well as an examination of a histogram of the data. These procedures were used for all statistical analysis. The equal variance assumption was confirmed using Levene's, Brown and Forsythe's, and Bartlett's tests [14]. An examination of the qq-plot of residuals and the residual versus predicted value plots was also used to evaluate the equal variance assumption [15]. All subsequent data sets in this paper fit these assumptions unless otherwise noted.

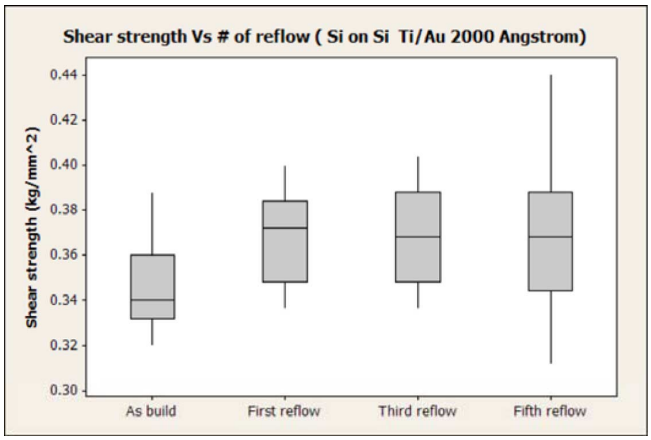

Fig. 9. Die shear strength as a function of reflows for Si on Si assembly (Ti/Au 2000 Å).

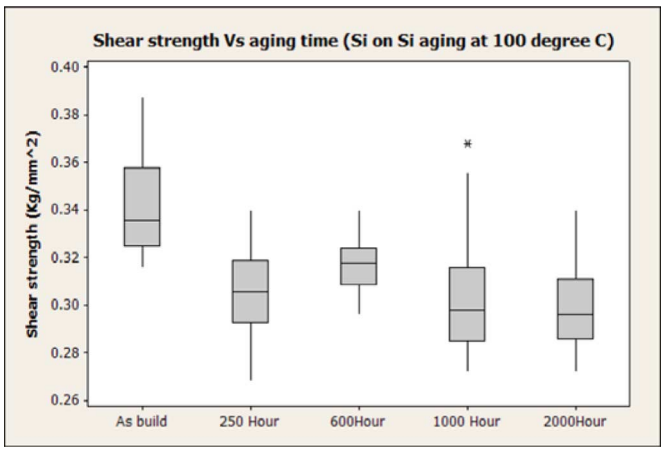

Fig. 10. Die shear strength as a function of aging (100 °C) for Si on Si assembly (Ti/Au 2000 Å).

The die shear test results as a function of aging at 100 °C are plotted in Fig. 10. The data trend is similar to the results with the TaN/Ru/Au backside Si die metallization [9]. The shear strength decrease ($\sim 10\%$) after 250 h aging was statistically significant after which the shear strength remained relatively constant through 2000 h. For the statistical analysis, the data was transformed using $1/(\text{shear strength})^{2.5}$ so the transformed data fit the normality assumption. The equal variance assumption was not satisfied, so to determine a difference among group means a Satterwaite F-test was used ($F_{5/114} = 12.4$, P-value $=<$ 0.0001) [16]. Differences between group means was determined using the least square means then adjusting for multiple comparisons using the Tukey criteria [17].

Thermal cycling is a concern for the heat spreader attachment due to the coefficient of thermal expansion (CTE) mismatch between Cu and Si. To evaluate this, Cu (24 mm $\times$ 24 mm) on Si (22 mm $\times$ 22 mm) test vehicles were assembled for air-to-air thermal shock testing. The test profile was from -40 °C to $+85$ °C, with 10 min at each temperature extreme and a transition time of 10 s. Figs. 11–14 are representative scanning acoustic microscopy (C-SAM) images taken during the thermal shock test. At 500 cycles, partial edge delamination was observed. The delamination grew slowly with additional cycles.

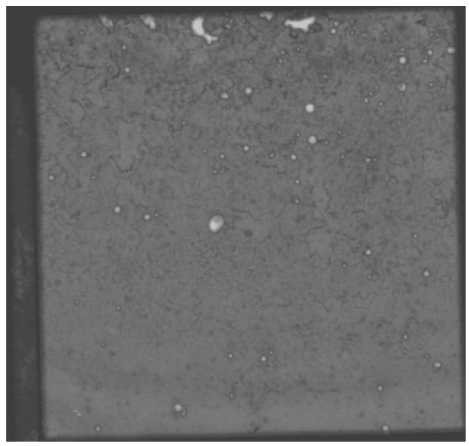

Fig. 11. C-SAM for assembly with Ti/Au (2000 Å) die before thermal shock cycles showing some voids, but no delamination. The die in the image is 22 mm $\times$ 22 mm.

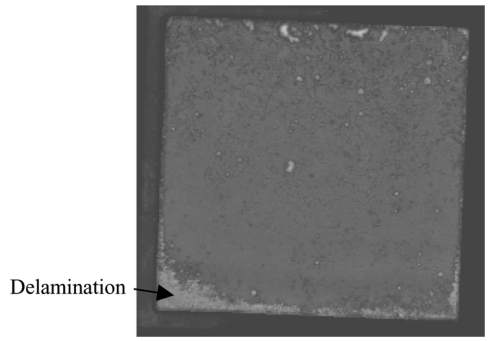

Fig. 12. C-SAM for assembly with Ti/Au (2000 Å) die after 500 thermal shock cycles showing delamination. The die in the image is 22 mm $\times$ 22 mm.

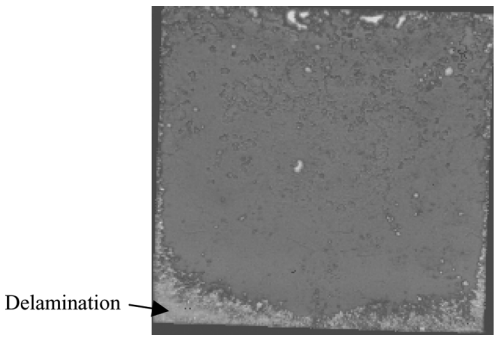

Fig. 13. C-SAM for assembly with Ti/Au (2000 Å) die after 1000 thermal shock cycles showing delamination. The die in the image is 22 mm $\times$ 22 mm.

Si (Ti/Ni/Au) had previously been evaluated for heat spreader attachment [18]. In that work, the air-to-air thermal shock test was from -55 °C to $+80$°C, a slightly wider temperature range. The Si die was 22 mm $\times$ 22 mm and the Cu heat spreader was 24 mm$\times$ 24 mm. After 2000 cycles, only slight edge delamination was found, which was much better than the Si (Ti/Au2000 Å) based assembly results in Fig. 14.

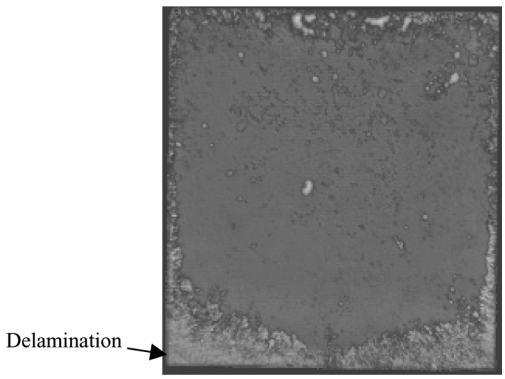

Fig. 14. C-SAM for assembly with Ti/Au (2000 Å) die after 2000 thermal shock cycles showing delamination. The die in the image is 22 mm × 22 mm.

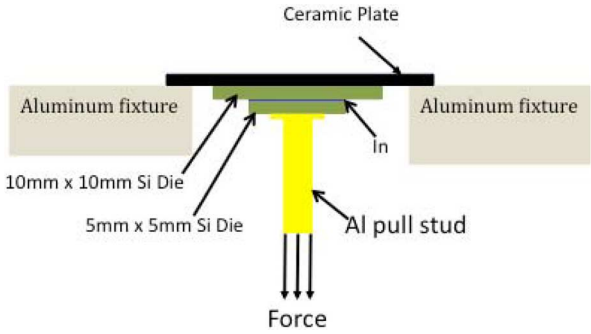

Fig. 15. Illustration of pull test showing ceramic plate used to reinforce the 10 mm× 10 mm Si die, the aluminum pull stud and the aluminum pull fixture.

C. Gold Thickness Effect for Ti/Au Metalized Die

To evaluate the effect of gold thickness on mechanical strength and failure mode, 5 mm × 5 mm Si on 10 mm × 10 mm Si samples were first built with different Au thicknesses and pull tested. The pull test is illustrated in Fig. 15. The bottom 10 mm × 10 mm Si die was attached to a ceramic plate to reinforce the Si. The ceramic plate was epoxy coated on one surface by the supplier. A clamp was used to clamp the part and the ceramic plate together during epoxy cure at 150 °C for an hour. The aluminum pull stud was then adhered to the top 5 mm × 5 mm Si die. The head of the aluminum pull stud was pre-coated with epoxy. A clamp was used to clamp the stud and the part with attached ceramic plate during epoxy cure at 150°C for an hour. The force-loading rate for the pull test was 0.45 kg/s.

The pull strength increased with the Au thickness (Fig. 16). To correct for the unequal variance a reciprocal transformation was performed on the data. An ANOVA F-test showed a difference between the group means. ($F_{4/45} = 61.95$, P-value $=<$ 0.0001). Tukey's pair wise test showed a statistical difference between the 500, 1000, 2000 and 3000 Å samples [17]. The difference between the 3000 and 4000 Å samples was not statistically significant at the 95% confidence level.

There was significant interfacial failure area (exposed Ti) for the assemblies with 500 Å and 1000 Å of Au. The dark areas in Figs. 17 and 18 are Ti.

For the 2000-Å Au assembly, a portion of the pull fracture surface was still at the Ti layer as seen from Fig. 19(a)–(c). The

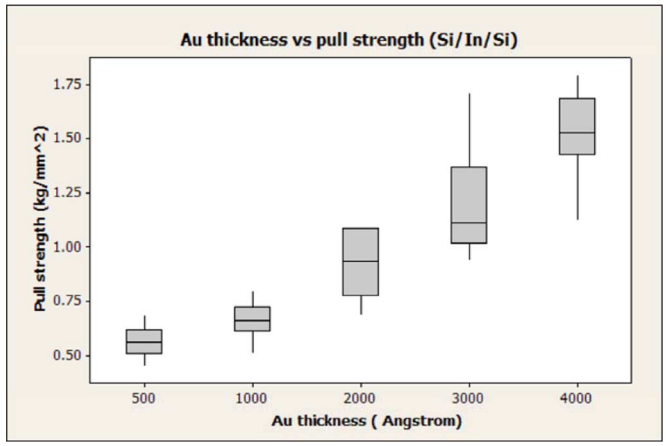

Fig. 16. Pull strength as a function of Au thickness for Ti/Au metallized Si die.

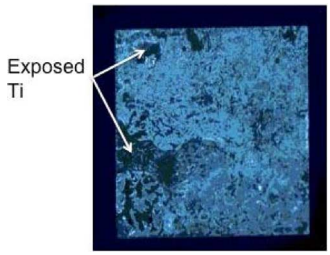

Fig. 17. Photograph of fracture surface after pull testing for Ti/500 Å Au test die. The die size is 5 mm × 5 mm.

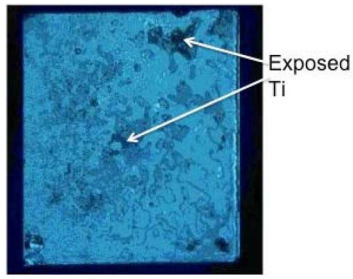

Fig. 18. Photograph of fracture surface after pull testing for Ti/1000 Å Au test die. The die size is 5 mm × 5 mm.

TABLE I
EDS "A", 2000 Å Au DIE FRACTURE SURFACE

Element	Line	keV	KRatio	Wt%	At%
O	KA1	0.523	0.0027	1.42	2.83
Si	KA1	1.740	0.6966	76.34	86.52
Au	MA1	2.121	0.0000	0.00	0.00
Ti	KA1	4.510	0.0976	11.58	7.70
In	LA1	3.286	0.0817	10.65	2.95
Total			0.8786	100.00	100.00

failure surface had Ti, but no Au as shown from Table I—EDS "A." The area labeled EDS "B" was In (Table II)

For the 3000-Å Au assembly, Fig. 20(a) is an X-ray image before pull and Fig. 19(b) is the pull fracture surface optical image. Corresponding voids are seen in both images. Some of the voids were though the thickness of the joint and were seen on

TABLE II
EDS "B," 2000 Å Au DIE FRACTURE SURFACE

Element	Line	keV	KRatio	Wt%	At%
O	KA1	0.523	0.0002	0.17	1.20
Si	KA1	1.740	0.0022	0.36	1.46
Au	MA1	2.121	0.0062	0.85	0.48
Ti	KA1	4.510	0.0004	0.05	0.12
In	LA1	3.286	0.9338	98.57	96.74
Total			0.9428	100.00	100.00

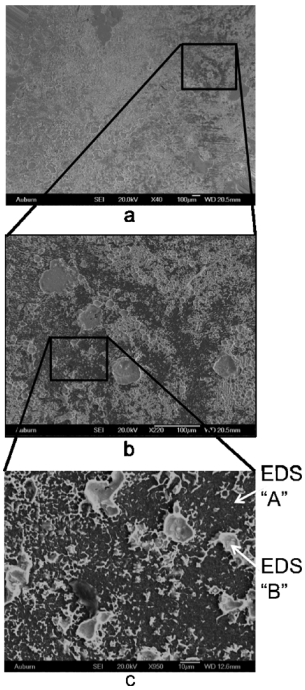

Fig. 19. SEM images for pull fracture surface for assembly with 2000-Å Au die: (a) x40, (b) x220, and (c) x950.

opposing pull fracture surfaces. Fig. 19(c)–(e) are the fracture surface SEM images.

The void surface had Ti but no Au (Table III—EDS "C"). Most of the remaining fracture surface was In as seen from EDS "D" and "E" (Tables IV and V). There were also some < 10 μm size failure surfaces (denoted as F). Higher Au and In composition were found at these sites as seen in EDS "F" (Table VI). This surface is physically close to the IMC (some Au, but more In was detected—the Au and In ratio did not correspond to $AuIn_2$).

For 4000-Å Au samples, Fig. 21(a)–(c) are the pull fracture surface SEM images. There were no large voids. Most of the fracture surface was In as seen from EDS "G" (Table VII). Other fracture surfaces (EDS "H") and (EDS "I") were closer to the IMC layer (some Au, but more In was detected (Tables VIII and IX).

The fracture surface composition analysis of the 4000-Å and 3000-Å Au assembles only showed minor differences with the exception of the larger voids. These voids resulted in localized noncontinuous IMC formation. For the 4000-Å assemblies, the IMC was found by TEM to be more continuous than the 3000-Å-based assembly. The 4000-Å pull fracture surface had little exposed Ti, even though some samples had slight voiding as determined by X-ray inspection.

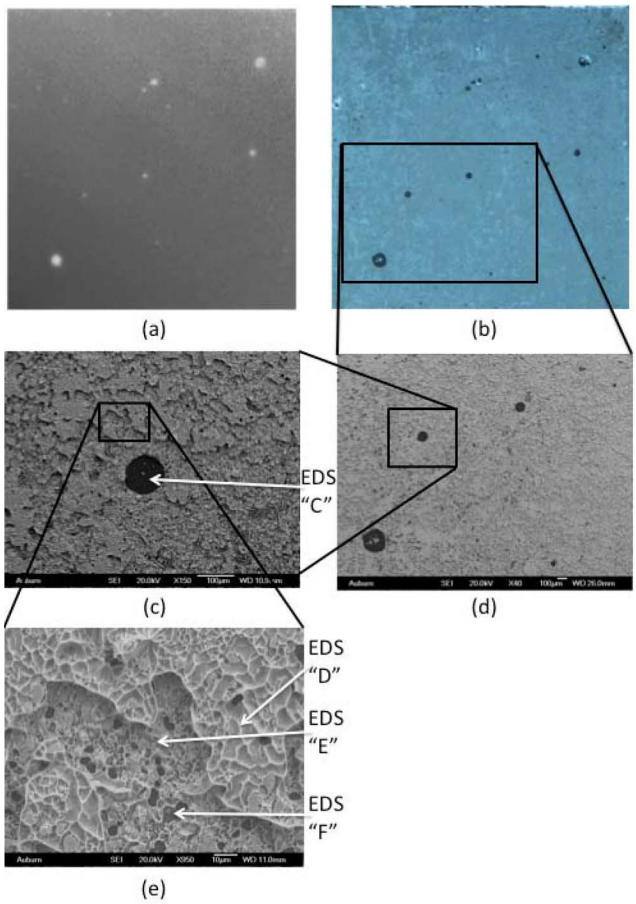

Fig. 20. (a) X-ray image for 3000-Å Au assembly. (b) Fracture surface optical image. (c) SEM x40. (d) SEM x150. (e) SEM x950.

TABLE III
EDS "C", 3000-Å Au DIE FRACTURE SURFACE

Element	Line	keV	KRatio	Wt%	At%
O	KA1	0.523	0.0000	0.01	0.02
Si	KA1	1.740	0.7983	84.47	91.04
Au	MA1	2.121	0.0000	0.00	0.00
Ti	KA1	4.510	0.1112	13.18	8.33
In	LA1	3.286	0.0177	2.34	0.62
Total			0.9273	100.00	100.00

TABLE IV
EDS "D", 3000-Å Au DIE FRACTURE SURFACE

Element	Line	keV	KRatio	Wt%	At%
O	KA1	0.523	0.0000	0.02	0.16
Si	KA1	1.740	0.0003	0.04	0.18
Au	MA1	2.121	0.0005	0.07	0.04
Ti	KA1	4.510	0.0000	0.00	0.00
In	LA1	3.286	0.9488	99.86	99.62
Total			0.9497	100.00	100.00

To further study the large voids, void analysis and its relationship with pull strength was evaluated for 3000-Å Au assemblies. The assemblies were inspected by X-ray for voids (Fig. 22). An image processing program was used to calculate the void area percentage. The pull strength as a function of void percentage is plotted in Fig. 23. The pull strength decreased as the void level increased. With minor voiding, the pull strength was close to

TABLE V
EDS "E", 3000-Å Au DIE FRACTURE SURFACE

Element	Line	keV	KRatio	Wt%	At%
O	KA1	0.523	0.0001	0.07	0.47
Si	KA1	1.740	0.0150	2.41	9.08
Au	MA1	2.121	0.0159	2.18	1.17
Ti	KA1	4.510	0.0098	1.14	2.52
In	LA1	3.286	0.8849	94.19	86.76
Total			0.9257	100.00	100.00

TABLE VI
EDS "F", 3000-Å Au DIE FRACTURE SURFACE

Element	Line	keV	KRatio	Wt%	At%
O	KA1	0.523	0.0000	0.00	0.00
Si	KA1	1.740	0.0031	0.49	2.20
Au	MA1	2.121	0.2022	27.06	17.38
Ti	KA1	4.510	0.0029	0.33	0.86
In	LA1	3.286	0.6249	72.12	79.56
Total			0.8330	100.00	100.00

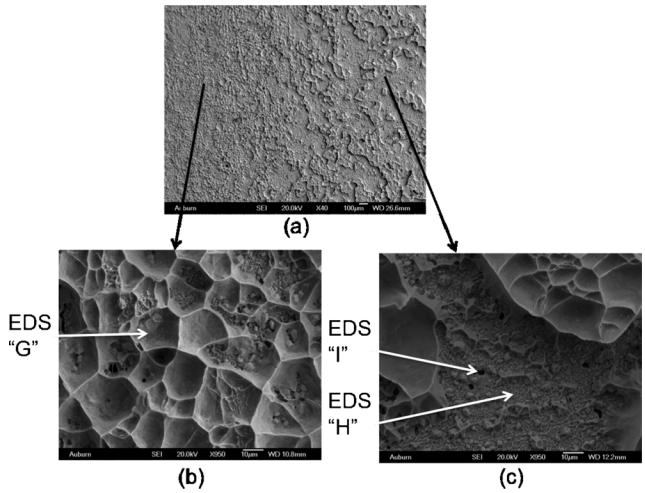

Fig. 21. SEM image for pull fracture surface for assembly with 4000-Å Au die: (A) X40, (B) X950, and (C) X950.

TABLE VII
EDS "G", 4000-Å Au DIE FRACTURE SURFACE

Element	Line	keV	KRatio	Wt%	At%
O	KA1	0.523	0.0001	0.13	0.91
Si	KA1	1.740	0.0009	0.15	0.60
Au	MA1	2.121	0.0026	0.36	0.20
Ti	KA1	4.510	0.0000	0.00	0.00
In	LA1	3.286	0.9431	99.37	98.29
Total			0.9468	100.00	100.00

TABLE VIII
EDS "H", 4000-Å Au DIE FRACTURE SURFACE

Element	Line	keV	KRatio	Wt%	At%
O	KA1	0.523	0.0000	0.00	0.00
Si	KA1	1.740	0.0006	0.09	0.41
Au	MA1	2.121	0.1963	26.30	17.15
Ti	KA1	4.510	0.0000	0.00	0.00
In	LA1	3.286	0.6403	73.62	82.45
Total			0.8372	100.00	100.00

that of the 4000-Å assemblies. It should be noted, the curve fit line should not be extrapolated to 0-kg pull strength at $\sim 10\%$

TABLE IX
EDS "I", 4000-Å Au DIE FRACTURE SURFACE

Element	Line	keV	KRatio	Wt%	At%
O	KA1	0.523	0.0001	0.08	0.57
Si	KA1	1.740	0.0033	0.53	2.21
Au	MA1	2.121	0.0671	9.13	5.41
Ti	KA1	4.510	0.0003	0.03	0.07
In	LA1	3.286	0.8327	90.23	91.74
Total			0.9034	100.00	100.00

Fig. 22. Example X-ray image showing voids. The die size is 5 mm × 5 mm.

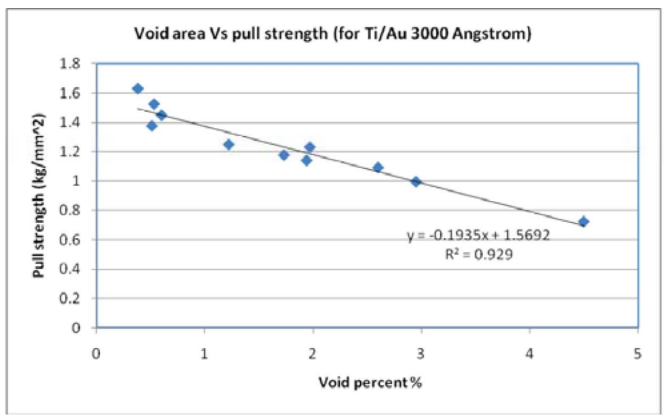

Fig. 23. Void area versus pull strength (for 3000-Å Au metallized die).

voiding. It is believed the voids are process related and not related to the Au thickness.

Shear strength was evaluated as a function of increasing gold thickness. Cu (10 mm × 10 mm) on Si (5 mm × 5 mm) samples were built and shear tested. Assemblies with 3000-Å and 4000-Å of Au had similar shear strength with shear failure in the bulk indium layer. Assemblies with 2000 Å of Au had lower shear strength (Fig. 24) and some samples showed significant Ti exposure in the fracture surface. Again an ANOVA F-test was used to determine if there was a difference between group means

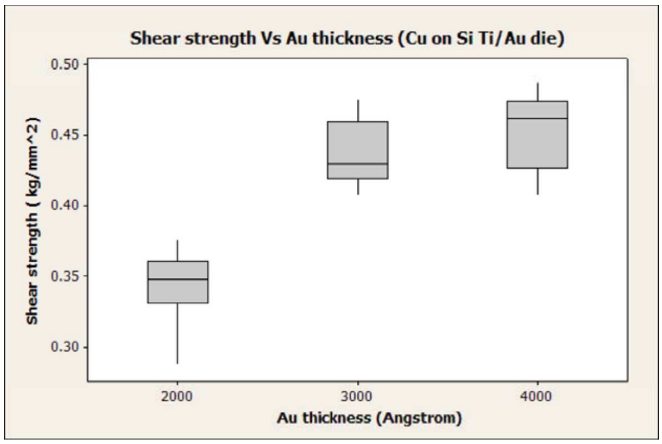

Fig. 24. Shear strength as a function of Au thickness for Ti/Au metallized Si Die.

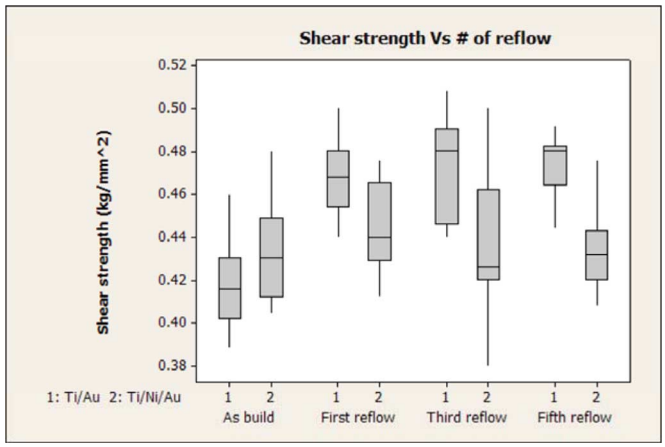

Fig. 25. Die shear strength as a function of number of reflows for Ti/Ni/Au and Ti/Au 3000-Å metallized die.

($F\neg_{2/27} = 57.39$, $P =< 0.0001$). Tukey's pair-wise test determined the difference between the 2000-Å samples and the 3000- and 4000-Å samples was statistically significant, while the difference between the 3000-Å and the 4000-Å samples was not.

With a flat Cu heat spreader attached, the solder joint is primarily in shear during the thermal shock test. Since 3000-Å Au and 4000-Å Au assemblies had similar shear strength, the decision was made to use Si die with 3000 Å of Au for the next series of tests. In volume production, the cost of the Au layer must be considered.

D. Heat Spreader Attach Reliability With Ti/Au 3000 Å and Ti/Ni/Au Metalized Die

Ti (1000 Å)/Au (3000 Å) and Ti (1000 Å)/Ni (2700 Å)/Au (1000 Å) metallized die were prepared. The Ti/Ni/Au die-based assembly was used as the control. To simulate a real product application, only Cu on Si was used in this part of the study. Cu (10 mm × 10 mm) on Si (5 mm × 5 mm) was used for multiple reflows and thermal aging tests. Cu (24 mm × 24 mm) on Si (22 mm × 22 mm) was used for thermal shock cycle tests.

The lead-free reflow test profile used was the same as in Fig. 7. The die shear strength as a function of multiple reflows for Ti/Ni/Au and Ti/Au metallized Si die is plotted in Fig. 25. A two-way ANOVA showed the statistical effect on mean shear strength was due to material type ($F_{1/68} = 15.21$, P-value $= 0.0002$), number of reflows ($F_{3/68} = 7.10$, P-value $= 0.0003$) and the interaction between the two variables ($F_{3/75} = 5.18$, P-value $= 0.0028$). Equal variance on the two-way data was confirmed using only the examination of the qq-plot of residuals and the residual versus predicted value plots, because the formal test results are not feasible for these data sets. Using Tukey's pair-wise test, there was no statistical significant difference in the as-built samples between Ti/Au and Ti/Ni/Au. There was a statistically significant difference (increase in shear strength) for the Ti/Au samples between as-built and after 1 to 5 reflows, while there was no statistically significant effect of reflow on the Ti/Ni/Au samples. The Ti/Au samples had higher mean shear strength (statistically significant) after multiple reflows compared to the Ti/Ni/Au.

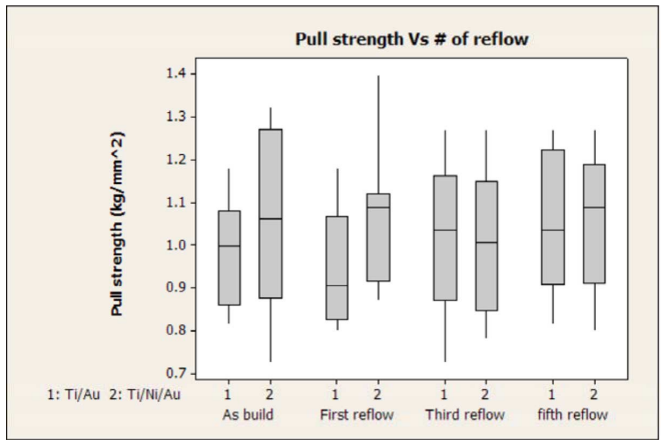

Fig. 26. Die pull strength as a function of reflows for Ti/Ni/Au and Ti/Au 3000-Å metallized die.

Die pull tests were performed on assemblies with the two die metallurgies after multiple reflows (Fig. 26). An ANOVA F-test showed no statistical effect due to material ($F_{1/72} = 1.63$, P-value $= 0.2059$), number of reflows ($F_{3/72} = 0.35$, P-value $= 0.7867$), or the interaction of the two ($F_{3/72} = 0.67$, P-value $= 0.5728$). The differences in pull strength were not statistically significant as a function of metallurgy or reflow cycles.

The thermal aging test was performed at 120 °C. Fig. 27 plots the shear test results after aging. A two-way ANOVA F-test showed no statistically significant difference in shear strength between Ti/Au and Ti/Ni/Au ($F_{1/72} = 1.76$, P-value $= 0.1893$), but there was a statistical effect on the group mean due to aging ($F_{3/72} = 3.10$, P-value $= 0.0049$) and the interaction between the two variables ($F_{3/72} = 3.86$, P-value $= 0.0127$). The difference in the Ti/Au sample between initial and after 1000 h at 120 °C was not statistically significant, while the difference between initial and after 1000 h at 120 °C was statistically significant for Ti/Ni/Au.

Die pull test were performed as a function of 120 °C aging (Fig. 28). There was no statistically significant variation in the pull strength as a function of aging for assemblies with either metallization. According to the two-way ANOVA F-test the

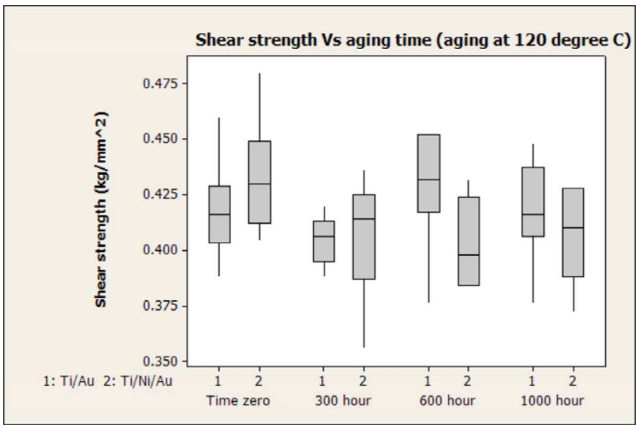

Fig. 27. Die shear strength as a function of aging at 120 °C for Ti/Ni/Au and Ti/Au 3000 Å metallized die.

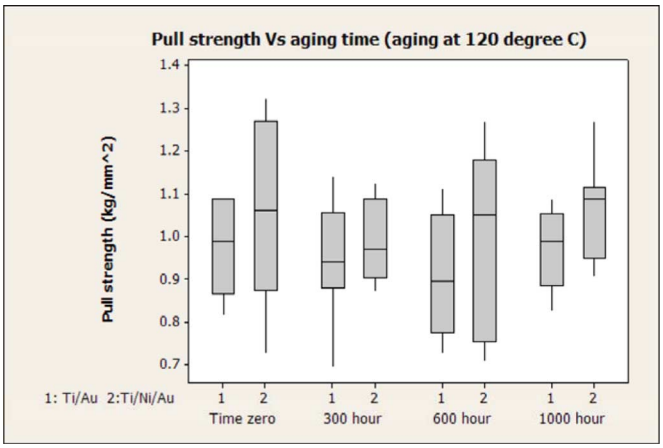

Fig. 28. Die pull strength as a function of aging at 120 °C for Ti/Ni/Au and Ti/Au 3000 Å metallized die.

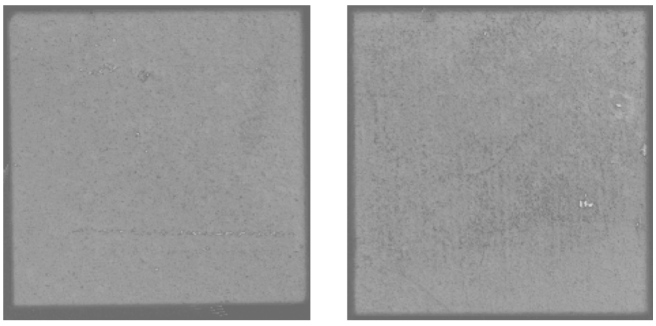

(a) (b)

Fig. 29. Typical C-SAM images for assemblies after 2X reflows. (a) TiAu and (b) Ti/Ni/Au showing some voiding, but no delamination. The die size is 22 mm × 22 mm.

mean pull strength of Ti/Ni/Au was slightly higher (statistically significant) than for Ti/Au. ($F_{1/72} = 4.69$, P-value $= 0.0337$)

The air-to-air thermal shock cycle test profile was from −40 °C to +85 °C, with 10-min dwells at each temperature extreme and a transition time of 10 s. Figs. 29–32 show examples of C-SAM images for assemblies after 2X lead free reflows then 500, 1000, and 2000 air-to-air thermal shock cycles. The assembly was Cu (24 mm × 24 mm × 1 mm) on Si (22 mm by 22 mm). There was no delamination for both Ti/Au and Ti/Ni/Au-based assembly after the initial 2X reflows (Fig. 29) or after 500 cycles (Fig. 30). After 1000 cycles, slight edge delamination was observed (Fig. 31) with both die metallurgies. The edge delamination occurred at the die–indium interface. After 2000 cycles, delamination progressed slightly with both die metallurgies (Fig. 32). There was little difference in the thermal shock results for assemblies with Ti/Ni/Au and Ti/Au (3000 Å) die. The delamination for the Ti/Ni/Au samples after 2000 cycles was comparable to the original test [18].

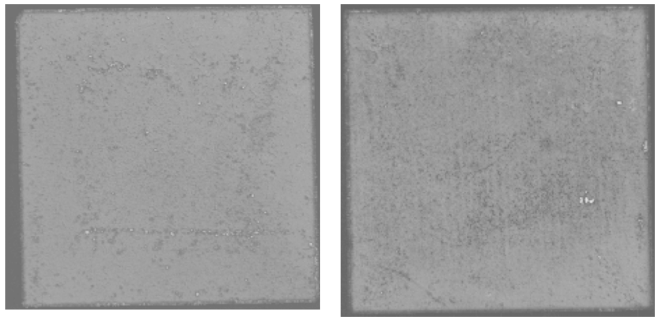

(a) (b)

Fig. 30. Typical C-SAM images for assemblies after 500 thermal shocks. (a) TiAu and (b) Ti/Ni/Au showing some voiding, but no delamination. The die size is 22 mm × 22 mm.

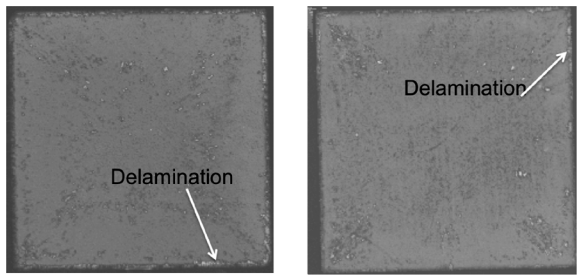

(a) (b)

Fig. 31. Typical C-SAM images for assemblies after 1000 thermal shocks. (a) TiAu and (b) Ti/Ni/Au showing some voiding and the beginning of edge delamination. The die size is 22 mm × 22 mm.

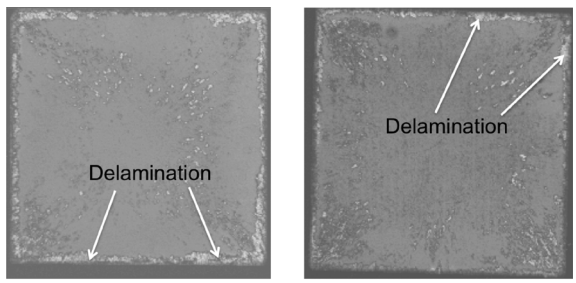

(a) (b)

Fig. 32. Typical C-SAM images for assemblies after 2000 thermal shocks. (a) TiAu and (b) Ti/Ni/Au Showing some voiding and increasing edge delamination. The die size is 22 mm × 22 mm.

II. Discussion

During initial assembly with the Ti/Au metallization, the Au is completely consumed and forms $AuIn_2$. During subsequent

high-temperature exposures (lead-free solder reflow and high-temperature aging) no additional intermetallic can form. The melting point of $AuIn_2$ is 539 °C and does not melt during lead-free reflow at 260°C. Lui, *et al.* reported very low wetting angles for In-to-$AuIn_2$ [19]. Thus, intermetallic growth or melting does not provide a mechanism for degradation during subsequent thermal exposure. The experimental die shear and pull tests after multiple reflow cycles and after thermal aging support this conclusion. Increasing the initial Au thickness produces a more continuous $AuIn_2$ layer. At 3000 Å, the $AuIn_2$ layer is nearly continuous. For thick 6-μm Au on Cu, Lui, *et al.* reported both a wavy, continuous $AuIn_2$ layer and floating islands of $AuIn_2$ in the In layer [19]. Given the much thinner Au layer in this work, **no** floating islands were observed in the as-fabricated samples. TEM and SEM analysis did not show $AuIn_2$ floating islands within the In layer even after high-temperature exposure as reported by [4] for Ni/Au metallization. The $AuIn_2$ remained adhered to the Ti layer. The larger voids in the Ti/Au (3000 Å), which corresponded to exposed Ti areas in the pull test fracture surfaces, are believed to be process induced voids and not specific to the 3000-Å Au samples. Without these voids, the pull strength of the 3000-Å Au samples was comparable to the 4000-Å Au samples. The primary failure mode for both Au thicknesses was ductile fracture of the In.

III. Conclusion

For indium soldering with Ti/Au thin film die metallization, the Au was consumed during soldering forming $AuIn_2$. There was no Ti–In IMC formation found; however, the attachment had good strength. The die shear and pull strength was not degraded significantly after multiple reflow or thermal aging.

Ti/Au (2000 Å) die-based Cu heat spreader attach (24 mm $\times$ 24 mm Cu on 22 mm $\times$ 22 mm Si) had early delamination during air-to-air thermal shock testing compared with Ti/Ni/Au die-based assembly.

With increasing Au thickness, the pull strength increased (Si on Si assembly). Ti/Au 2000 Å had significant exposed Ti at the pull failure surface. Ti/Au (3000 Å) assembly had a small percentage of voids that exposed Ti in the pull failure surface. The voids degrade the assembly pull strength compared with Ti/Au (4000 Å). Ti/Au (3000 Å) (Cu on Si) and Ti/Au (4000Å) had similar shear strength, while Ti/Au (2000 Å) had lower shear strength.

Ti/Au (3000 Å) die-based Cu heat spreader attach had multiple reflow, thermal aging and thermal shock reliability comparable to Ti/Ni/Au metallized Si die. Ti/Au is a viable die backside metallization for Cu heat spreader attachment with In solder.

References

[1] "Developments and trends in thermal management technologies—A Mission to the USA report of a DTI global watch mission," 2006.

[2] Y. Li, R. W. Johnson, P. Thompson, T. Hooghan, and J. Libres, "Reliability of flip chip packages with high thermal conductivity heat spreader attach," in *Proc. IEEE 58th Electron. Compon. Technol. Conf.*, May 27–28, 2008, pp. 2011–2017.

[3] Hua, Fay, Deppisch, Carl, Fitzgerald, and Tom, "Indium as thermal interface material for high power devices," *Adv. Microelectron.*, pp. 16–17, Jul./Aug. 2006.

[4] Deppisch, Carl, Fitzgerald, Thomas, Raman, Arun, Hua, Fay, Zhang, Charles, Liu, Pilin, Miller, and Mikel, "The material optimization and reliability characterization of an indium-solder thermal interface material for CPU packaging," *JOM J. Minerals, Metals, Mater. Soc.*, vol. 58, no. 6, pp. 67–74, Jun. 2006.

[5] Too, S. Sean, Touzelbaev, Maxat, Khan, Mohammad, Master, Raj, Diep, Jacquana, Keok, and Kee-Hean, "Indium thermal interface material development for microprocessors," in *Proc. 25th Annu. IEEE Semicond.Thermal Meas. Manage. Symp., SEMI-THERM 2009*, Mar. 15–19, 2009, pp. 186–192.

[6] H. Zhang, Y. C. Mui, Poh-Eng, Tan, Soon-Hwa, and Ng, "Thermal characterizations of solid thermal interface materials," in *Proc. 10th Electron. Packag. Technol. Conf., EPTC 2008*, Dec. 9–12, 2008, pp. 1472–1478.

[7] Chaowasakoo, Tanawan, Ng, T. Hoon, Songninluck, Jinda, Stern, B. Margaret, Ankireddi, and Sai, "Indium solder as a thermal interface material using fluxless bonding technology," in *Proc. 25th Annu. IEEE Semicond. Thermal Meas. Manage.t Symp., SEMI-THERM 2009*, Mar. 15–19, 2009, pp. 180–185.

[8] R. Darveaux and I. Turlik, "Shear deformation of indium solder joints," *IEEE Trans. Compon., Hybrids, Manuf. Technol.*, vol. 13, no. 4, pp. 929–939, Dec. 1990.

[9] S. Sivaswamy, R. Wu, C. Ellis, M. Palmer, R. W. Johnson, P. McCluskey, and K. Petrarca, "System-in-Package for extreme environments," in *Proc. Electron. Compon. Technol. Conf.*, 2008, pp. 2044–2050.

[10] G. Humpston and D. Jacobson, *Principles of Soldering*. Materials Park, OH: ASM International, 2004, pp. 53–53.

[11] F. L. Ramsey and D. W. Schafer, *The Statistical Sleuth*. Pacific Grove, CA: Duxbury, 2002, pp. 122–130.

[12] S. S. Shapiro, M. B. Wilk, and H. J. Chen, "A comparative study of various tests for normality," *J. Amer. Statist. Assoc.*, vol. 63, no. 324, pp. 1343–1372, 1968.

[13] M. A. Stephens, "EDF statistics for goodness of fit and some comparisons," *J. Amer. Statist. Assoc.*, vol. 69, no. 347, pp. 730–737, 1974.

[14] M. B. Brown and A. B. Forsythe, "Robust tests for the equality of variances," *J. Amer. Statist. Assoc.*, vol. 69, no. 346, pp. 364–367, 1974.

[15] F. L. Ramsey and D. W. Schafer, *The Statistical Sleuth*. Pacific Grove, CA: Duxbury, 2002, pp. 131–133.

[16] J. M. Davenport and J. T. Webster, "A comparison of Some Approximate F Tests," *Technometrics*, vol. 35, no. 4, pp. 779–790, 1973.

[17] M. R. Stoline, "The status of multiple comparisons: Simultaneous estimation of all pairwise comparisons in one-way ANOVA designs," *The American Statistician*, vol. 35, no. 3, pp. 134–141, 1981.

[18] F. Ding, "Flip chip and lid attachment assembly process development," Ph.D., Auburn Univ., Auburn, AL, 2006.

[19] Y. M. Liu and T. H. Chuang, "Interfacial reactions between liquid indium and Au-deposited substrates," *J. Electron. Mater.*, vol. 29, no. 4, 2000.

Yuquan Li received the B.S. and M.S. degrees in electrical engineering from Ocean University of China, Qingdao, in 1999 and 2002 respectively, and the Ph.D. degree in semiconductor packaging from Auburn University, Auburn, AL, in 2009.

He did an internship with Freescale Semiconductor during his study and he is now a package development engineer with ACAMP (Alberta Centre for Advanced MNT Products).

R. Wayne Johnson (S'85–M'97–SM'94–F'04) received the B.E. and M.Sc. degrees from Vanderbilt University, Nashville, TN, in 1979 and 1982 and the Ph.D. degree from Auburn University, Auburn, AL, in 1987, all in electrical engineering.

He is a Professor of Electrical Engineering at Auburn University and Director of the Laboratory for Electronics Assembly and Packaging (LEAP). Current research projects include lead-free electronics assembly, mixed lead-free and Sn/Pb electronics assembly, wafer-level packaging, flip chip assembly, assembly of ultra-thin Si die, and electronics packaging for extreme environments (−230 °C to +485 °C).

Prof. Johnson is a Fellow of the International Microelectronics Packaging Society, a member of the Surface Mount Technology Association (SMTA), and the IPC (Association Connecting Electronics Industries). He is Vice President of Publications for the IEEE Components, Packaging and Manufacturing Technology (CPMT) Society Board of Governors. He is also Editor-in-Chief of the IEEE TRANSACTIONS ON ELECTRONICS PACKAGING MANUFACTURING.

Rui Zhang received the B.S. degree in electrical engineering from Tsinghua University, Beijing, China, in 2006, and the M.E.E. degree in electrical engineering from Auburn University, Auburn, AL, in 2009. He is currently pursuing the Ph.D. degree in the Laboratory for Electronics Assembly and Packaging (LEAP), Auburn University.

His research interests include hybrid electronics, flip chip technology, and high-temperature packaging.

Mr. Zhang is a student member of IMAPS.

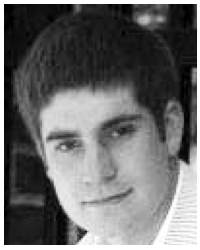

Phillip Henson received the B.S. degrees in electrical engineering and materials engineering from Auburn University, Auburn, AL, in 2008. Currently he is pursuing the M.S. degree in electrical engineering at Auburn University.

His research interests are in high-temperature electronics packaging, mainly die attach and wire bond materials.

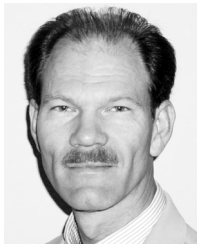

Patrick Thompson (SM'92) received the B.S., M.S., and Ph.D. degrees in chemical engineering from the University of Missouri-Rolla in 1979, 1981, and 1983, respectively.

He has spent more than 25 years in the area of advanced packaging research, development, and transfer to manufacturing. He has led development teams at Bell Labs, AMI Semiconductors, and Motorola (now Freescale), working on technologies ranging from flip chip fabrication and packaging, flip chip-on-board to chip-scale packages, multi-chip packaging, MEMS, and optoelectronic packaging. Since 2001, he has been a Senior Member of the Technical Staff at Texas Instruments, Dallas, TX, where he is currently Lead Technologist on fine-pitch flip chip technology development. He has five patents and over two dozen publications.

He is a Senior member of the American Society for Quality. He is active in industry–consortia and industry–university partnerships.

Tejpal Hooghan received the M.S. degree in materials science and the Ph.D. degree in physics from the University of North Texas, Denton, in 1996 and 1997, respectively.

She worked as a Research Scientist at Baylor College of Dentistry, Dallas, TX, to continue her research in dental materials. In 1998, she started a position in packaging with Lucent Technologies (Bell Labs) where she worked on early development of Cu and low-k dielectric and interaction with packaging and first generation of flip chip packages. She transitioned to optical packaging development at Lucent in 2000. She worked at Lehigh University, Bethlehem, PA, as a Visiting Scientist for one year where she worked on energy filters designed to improve EBSD patterns. In 2004, she moved to Texas to take a Packaging Engineer position at Texas Instruments, Dallas. She designed and qualified new silicon high-performance flip chip packages. Her expertise is in materials characterization and microstructural analysis using electron beam techniques.

Jeremias Libres received the B.S. degree in mechanical engineering from Saint Louis University, Baguio, Philippines, and the M.S. degree in mechanical engineering from Southern Methodist University, Dallas.

He is a Member Group Technical Staff in the Flip Chip Packaging Group in the Semiconductor Packaging organization of Texas Instruments, Dallas, TX. He is responsible for platform development and ramp of next-generation Pb-free ceramic flip chip packages, which includes development and qualification of new underfills, thermal interface materials, and substrate technologies. Prior to this assignment, he has worked in various roles and strategic projects in the company, which includes Pb-free package development for large-body ceramic packages, molded organic flip chip BGAs, film-assist transfer molding technology, and process engineering in the IC assembly operations. He is author/coauthor of a number of technical papers and patents related to flip chip packaging and encapsulation process technologies.